

Atomic-scale study of Si-doped AlAs by cross-sectional scanning tunneling microscopy and density functional theory

D. Tjeertes^{1,*}, A. Vela², T. J. F. Verstijnen¹, E. G. Banfi¹, P. J. van Veldhoven¹,
M. G. Menezes², R. B. Capaz², B. Koiller², and P. M. Koenraad¹

¹*Department of Applied Physics, Eindhoven University of Technology, P.O. Box 513, 5600 MB Eindhoven, Netherlands*

²*Instituto de Física, Universidade Federal do Rio de Janeiro, Caixa Postal 68528, 21941-972 Rio de Janeiro, RJ, Brazil*



(Received 14 June 2021; revised 7 September 2021; accepted 14 September 2021; published 24 September 2021)

Silicon (Si) donors in GaAs have been the topic of extensive studies since Si is the most common and well understood *n*-type dopant in III-V semiconductor devices and substrates. The indirect band gap of AlAs compared to the direct one of GaAs leads to interesting effects when introducing Si dopants. Here we present a study of cross-sectional scanning tunneling microscopy and density functional theory (DFT) calculations to study Si donors in AlAs at the atomic scale. Based on their crystal symmetry and contrast strengths, we identify Si donors up to four layers below the (110) surface of AlAs. Interestingly, their short-range local density of states (LDOS) is very similar to Si atoms in the (110) surface of GaAs. Additionally, we show high-resolution images of Si donors in all these layers. For empty state imaging, the experimental and simulated STM images based on DFT show excellent agreement for Si donors up to two layers below the surface.

DOI: [10.1103/PhysRevB.104.125433](https://doi.org/10.1103/PhysRevB.104.125433)

I. INTRODUCTION

In the past few years, cross-sectional scanning tunneling microscopy (X-STM) has become the primary tool for performing spatial analysis of electronic wave functions of point defects in semiconductors [1]. In this respect, silicon (Si) defects in III-V compounds are particularly interesting, since Si is the most common *n*-type dopant in these systems. In particular, the extensively studied III-V compound GaAs is a direct band-gap semiconductor, therefore Si donor states have strong contributions from the GaAs conduction band minimum at the Γ point. The (110) surface of Si-doped GaAs has been well studied using X-STM [2–8]. Signatures of Si atoms in GaAs in different charge states have been identified, and control of the charge state of surface Si donors with the STM tip and laser illumination has been shown, where the donor switches from a negative charge to a positive charge and vice versa [9]. Si atoms below the (110) surface of GaAs are shallow donors. At large negative bias, they are in a neutral state (d^0) and at large positive bias they become ionized due to tip-induced band bending (TIBB), visible as rings of ionization [6], leading to a positively charged donor (d^+). A schematic visualization of the TIBB can be found in Fig. S14 of the Supplemental Material [10]. Si atoms at the (110) surface of GaAs can switch between a donorlike state similar to Si atoms below the surface, and a deep DX^- like state [8,11]. In the DX^- -like state, the Si atom undergoes a bond reconfiguration and is negatively charged ($d^+ + 2e^-$) with an extra electron occupying the dangling bond.

Another paradigmatic and technologically important example of a shallow donor in semiconductors is a phosphorus

(P) donor in Si, where the bottom of the conduction band does not lie at the center or at an edge of the Brillouin zone (BZ), but instead is located at a point on the Δ line in the BZ roughly 85% from Γ to X . The band structure then presents a sixfold degenerate conduction band minimum, as there are six nonequivalent Δ directions. The coupling among the six degenerate minima by the donor perturbation potential gives rise to interference patterns in the defect wave function [12]. These can be identified by STM [13–17] in the (001) surface as alternating patterns, on a four-layer cycle, depending on the impurity depth from the surface [18].

Si donors in AlAs represent an interesting intermediate situation between the two aforementioned cases, as AlAs, like Si, is an indirect gap material, but the conduction band minimum is at X point, i.e., at the BZ boundary. The X valley is threefold degenerate (X_x , X_y , and X_z), so the donor electron imaging on a (110) surface could potentially reveal new symmetry features with respect to donors in direct gap materials, like GaAs, and sixfold-degenerate indirect gap materials, like Si. There is relatively little literature on Si doping of pure AlAs, but around the 1990s, superlattices of Si doped AlAs and GaAs were of interest for the development of laser structures [19], which included research into the donor ionization energy [20] and carrier recombination [21] in these superlattices and the effects of Si atoms close to the AlAs and GaAs interfaces. The results of these studies do not provide direct insight into the properties of Si donors in pure AlAs since the superlattice periodicity was smaller than the donor Bohr radius of the Si atoms, causing overlap with the GaAs layers. Here we present a study of Si donors at various depths below a (110) surface of bulk *n*-type AlAs.

Our X-STM results are supported by electronic structure calculations. Several theoretical methods have been successfully used in the past to simulate STM images, providing a

*d.tjeertes@tue.nl

direct bridge between theory and experiment. Density functional theory (DFT) is often the preferred tool because it incorporates an *ab initio* description of electronic structure (including electronic correlation effects) and full relaxation of atomic coordinates, which is important when studying defects and surfaces. DFT has been used in the past to simulate STM images for reasonably deep (strongly localized) defects [22], where relatively small supercells can be used. For shallow defects in semiconductors, like Si donors in GaAs (Bohr radius ≈ 100 Å) or even P donors in Si (average Bohr radius ≈ 19 Å, estimated using the geometric mean of transverse and longitudinal effective masses), the bound electron wave function extends over many lattice parameters, requiring supercell sizes beyond current DFT size limits. In this case, semiempirical methods such as tight-binding [23] or those based on the effective-mass theory [24] (combining DFT bulk states forcefully modulated by an empirical envelope function) [18], can sometimes provide a good qualitative or semiquantitative description of STM measurements as cuts of the bulk wave functions, without the explicit inclusion of surface relaxation or surface states.

In this paper, Si donors at different depths below the (110) surface of AlAs are identified in X-STM and their signatures are confirmed by DFT calculations. The relatively smaller AlAs average donor Bohr radius of 13 Å (also estimated using the geometric mean of effective masses [25]) allows us to obtain reliable simulated images using fully *ab initio* DFT calculations, which explicitly include atomically relaxed surfaces. We obtain excellent agreement between X-STM measurements and DFT calculated images. We combine these techniques to study donors in III-V compounds.

II. METHODS

A Si-doped AlAs sample was grown using molecular beam epitaxy on an n^+ -doped (001) GaAs substrate. The sample contained (in the growth direction) a 100-nm undoped GaAs buffer, 50 nm of intrinsic AlAs, 400 nm of AlAs with 1×10^{18} cm $^{-3}$ Si doping, a 50-nm intrinsic AlAs layer, and a 200-nm intrinsic GaAs capping. The main purpose of the GaAs capping is to prevent the oxidation of the highly reactive AlAs layers.

For X-STM measurements, the samples are brought into the ultrahigh vacuum STM chamber (typical pressure below 5×10^{-11} mbar) and cleaved *in situ*, revealing one of the {110} planes of the sample. This allows us to image a cross section of the sample showing all the grown layers. All measurements were performed at 77 K in an Omicron LT-STM in constant current mode. STM tips were electrochemically etched from polycrystalline tungsten (W) wire and further tip preparation was done by sputtering with argon (Ar). STM images have their contrast adjusted individually to optimize the visibility of the features. The typical height of the atomic corrugation is 20 to 50 pm, depending on the tunneling conditions.

Our DFT calculations were performed in two steps. Initially, for smaller cells, we employ the QUANTUM ESPRESSO suite (QE) [26,27], that uses a plane-wave basis to expand the electronic wave functions (energy cutoffs of 30 Ry for the wave functions and 240 Ry for the density). We use the local

density approximation (LDA) [28–30] to describe exchange and correlation effects and ultrasoft pseudopotentials [31–33] for electron-ion interactions. The equilibrium lattice constant of bulk AlAs given by our calculations is 5.67 Å, in excellent agreement with experimental data. This value is employed in all subsequent calculations. The AlAs(110) surface is modeled by an 11-layer slab with a vacuum layer of 12 Å to isolate the slab from its vertical periodic images. A 3×4 supercell (264 atoms) of the original surface unit cell is used to accommodate the Si impurity and isolate it laterally from its periodic images. Then a Monkhorst-Pack sampling [34] of $3 \times 2 \times 1$ is employed. All atomic coordinates are fully relaxed with a force tolerance of 10^{-3} Ry/Bohr and then used as reference for constructing the initial atomic positions in the second part of the calculations, performed with the SIESTA code [35]. These calculations allow us to use larger supercells that provide an improved description of the extension and the energetics of the shallow impurity states. Additionally, notice that this two-step procedure reduces the computational cost of the structural optimization in larger supercells by including the effects of surface reconstruction and local modifications induced by the impurity from the start.

In SIESTA, the wave functions are expanded in a pseudoatomic double zeta polarized orbital basis, with a mesh cutoff of 300 Ry. Norm-conserving pseudopotentials were used for the ion-electron interaction and a LDA - Perdew-Zunger exchange-correlation functional was used for the electron-electron interaction [36,37]. The (110) surface is modeled by a slab supercell consisting of 12 atomic layers, following the labeling in Fig. 1. The surface supercell is now 6×8 (six zigzag chains along the [001] direction and each chain containing 16 atoms along the $[\bar{1}10]$ direction), resulting in a total of 1152 atoms. Additionally, a vacuum of 20 Å is included. All atomic positions are allowed to relax until forces are smaller than 0.04 eV/Å and the BZs were sampled by a $2 \times 2 \times 1$ Monkhorst-Pack k-point grid [34]. All calculations discussed throughout the text come from this second step, unless explicitly stated otherwise.

We simulate constant-height STM images at 2 Å above the surface for all the systems using the Tersoff and Hamann approach [38]. To visualize the defect-level wave functions, the local density of states (LDOS) is integrated over narrow energy windows that include only the defect state. In QE, the windows range from -0.18 to -0.11 eV, measured from the Fermi energy, depending on the defect position. Similar windows are employed in SIESTA's calculations.

III. RESULTS AND DISCUSSION

A. {110} surface states of III-V semiconductors

Before presenting our results on the X-STM images of Si defects, it is interesting to review the knowledge of (110) surface states of III-V compounds, as they will set the background of defect-state images and help us with the detailed description of the structural and electronic features of those defects. The atomic corrugation observed with STM on {110} surfaces of III-V semiconductors is related to a number of surface resonances, located on either side of the band gap as schematically shown in Fig. 1(c) [39,40]. The C_3 and C_4 states

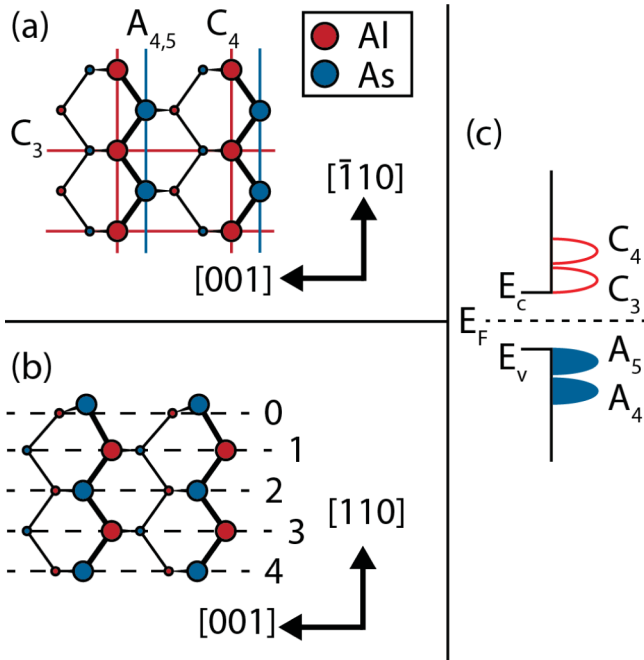


FIG. 1. (a) Schematic top view of an AlAs (110) surface, with Al and As atoms colored red and blue, respectively. The A_4 and A_5 surface states are indicated schematically with blue lines, and the C_3 (horizontal) and C_4 (vertical) are marked with red lines. Atoms located one layer below the surface are depicted smaller. (b) Schematic side view of the (110) AlAs surface. Layers are labeled numerically, starting with the surface as 0. In the top layer, the characteristic buckling is depicted. (c) A schematic energy diagram of the surface states of an undoped III-V semiconductor with no band bending, where E_c , E_F , and E_v indicate the conduction band, Fermi level, and valence band energy, respectively

are located in the conduction band just above the band edge, while the A_4 and A_5 states are located in the valence band, just below the band edge. At large negative voltages, the contrast in the STM images results from both A_4 and A_5 states. These states are constructed from particular combinations of atomic orbitals located on the anion sublattice [39] and they both appear as rows running perpendicular to the [001] crystal axis [40], as shown schematically in Fig. 1(a). In this figure, the anion (As) atoms are shown as blue disks and the A_4 and A_5 states are represented by blue lines. Since these particular combinations of anion orbitals appear as being connected in the $[\bar{1}10]$ direction, the image will display a series of rows along this particular direction. Shifting to smaller negative voltages moves the A_4 state below the tip Fermi level, leaving only the A_5 state which still shows, by itself, a 1D row pattern along $[\bar{1}10]$ in the STM images. At even smaller negative voltages, the contribution of the C_3 state becomes relevant. The C_3 state contributes to the tunneling at negative voltages due to TIBB pulling it below the Fermi level, but it only contributes significantly at small negative voltages because the contribution from the A_5 states is very weak. The C_3 states are composed of p -like cation dangling bonds nearly parallel to the [001] crystal axis [39] and therefore they contribute to STM images as 1D rows along [001], as shown schematically in Fig. 1(a). Therefore, for small negative voltages, the

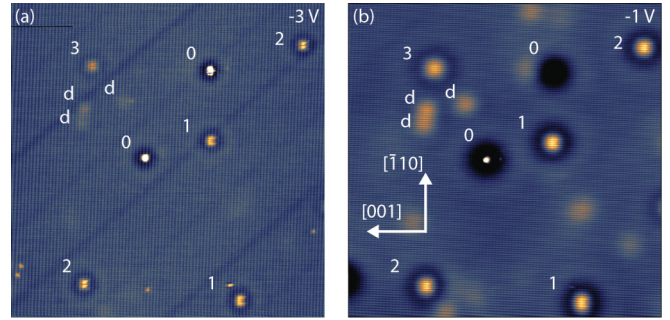


FIG. 2. $50 \times 50 \text{ nm}^2$ filled state images obtained at two different voltages (a) -3 V , (b) -1 V containing multiple features. The numbers 1–3 mark Si donors one, two, and three layers below the surface, respectively. The letters d mark Si donors located deeper below the surface and the numbers 0 mark surface defects/donors. Friedel oscillations are visible around the features and increase in amplitude when going from larger (a) to smaller (b) negative voltages. Both images were obtained with a current set point of 30 pA.

combined contribution of both A_5 and C_3 states gives rise to corrugation along both $[\bar{1}10]$ and [001] directions, i.e., 2D atomic corrugation. At small positive bias, the C_3 state has the largest contribution to the tunnel current, resulting in a 1D corrugation running over the cation sublattice in the [001] direction. At larger positive voltages, the C_4 states start to contribute and they are composed of combinations of cation atomic orbitals that appear in STM images as rows along the $[\bar{1}10]$ direction, as indicated by the corresponding red line in Fig. 1(a). The STM images at these large positive voltages contains contributions from both the C_3 and C_4 states, resulting in a 2D corrugation on the cation sublattice. The exact voltages at which these surface states contribute most strongly depend on the work function of the tip, but their relative positioning with regard to voltage remains the same.

The side view of the cleaved (110) surface is shown in Fig. 1(b). The layers are labeled numerically starting with the surface layer as 0 and increasing going deeper into the bulk. We adopt this labeling in all following sections. Notice that the side view is very similar to the top view, with the main difference being in the surface layer, that shows schematically the typical buckling of the (110) surface of III-V semiconductors [41–43], where the anions move slightly out of the surface compared to their ideal position, while the cations move slightly into the bulk.

B. X-STM

Figure 2(a) shows a filled-state STM image obtained on Si doped AlAs at a bias voltage of -3 V and tunnel current of 30 pA. The $A_{4,5}$ surface states can be observed as rows of bright contrast in the $[\bar{1}10]$ direction. A single low-frequency noise can be observed running diagonally through the image, from the bottom left to the top right. Figure 2(b) shows the same area as Fig. 2(a) but the bias voltage has been changed to -1 V . The background contrast now consists of mainly C_3 states running in the [001] direction and the low frequency noise has disappeared. In both images, a multitude of features can be observed, which will be described and classified in the following section, based on symmetry arguments and the

strength of their contrast. With symmetry arguments, it can be determined if a donor is located in an even or odd layer below the surface. Si donors will substitute an Al atom, and looking at Fig. 1(b) it can be seen that in even layers (2, 4, etc.) the Al lattice sites are located directly below the surface Al sites. In odd layers (1, 3, etc.), they are located in between the Al sites instead. As explained before, at positive bias the Al sublattice is imaged, due to the C_3 and C_4 surface states. If a donor is now located in an even layer, it should have a mirror axis in the [001] direction which lies *on* a C_3 state. If the donor is located in an odd layer, its [001] mirror axis should be located *in between* two C_3 states. This technique has been employed before to determine the layer in which features are located in STM measurements [44,45]. The strength of the contrast of donor atoms in GaAs has been shown to reduce and become less localized when they are located deeper below the surface [2,45].

1. Identification of features based on the strength and symmetry of the contrast

Si donors below the surface are marked with the numbers 1–3, referring to their respective layers, using the labels from Fig. 1(b). The letter d indicates Si donors deeper below the surface. The number 0 indicates either Si donors at the surface layer or other types of surface defects, which are difficult to distinguish at filled-state imaging due to their very strong and localized contrast, often resulting in a convolution of the feature with the STM tip. The donors marked by 1 and 2 show a central bright contrast with a dark ring surrounding it, which in turn is surrounded by a weaker bright contrast ring. The wavelength and amplitude of these oscillations increase at smaller negative voltages, as can be seen when comparing Figs. 2(a) (–3 V) and 2(b) (–1 V). These concentric rings have been attributed to charge density (Friedel) oscillations [46].

TIBB can, during filled-state imaging, pull the conduction band states below the Fermi level, causing an accumulation layer at the surface as schematically shown in Fig. S14 of the Supplemental Material. This accumulation layer can be treated as a two-dimensional electron gas (2DEG), in which the Si donors act as impurities which will be screened by this 2DEG, resulting in long-range Friedel oscillations. The increase in amplitude and wavelength of the oscillations when going from large negative voltage to smaller negative voltages can be explained by the band bending. Imaging at smaller negative voltages reduces the TIBB, resulting in a local decrease of the electron density and the corresponding reduction of the distance between the Fermi energy and the bottom of the conduction band. Since the wavelength of the oscillations is proportional to the Fermi wavelength, it should increase with decreasing Fermi energy. The reduced band bending also decreases the amount of states below the Fermi energy that contribute to the tunneling current, meaning that the contribution of the electrons around the Fermi energy has increased relatively to the background, resulting in a larger amplitude of the oscillations [47]. The closer the donor is located to the surface, the stronger these oscillations will be [48].

With this information, it is also possible to determine the relative depth of the donors observed in Figs. 2(a) and 2(b).

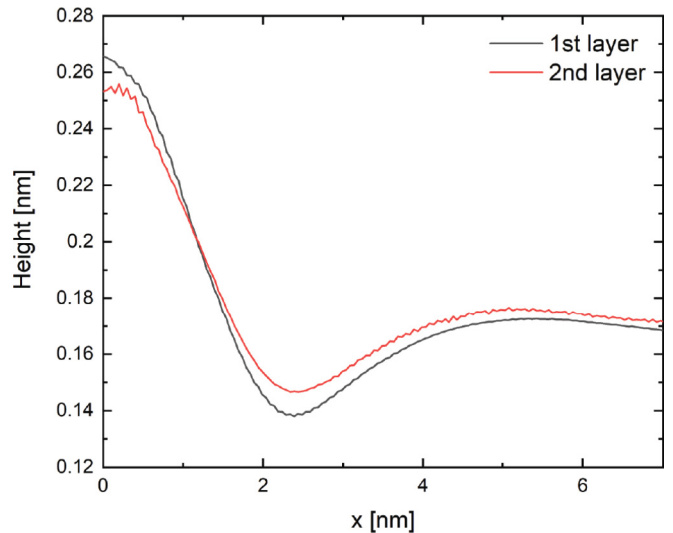


FIG. 3. Radial height profiles of first- and second-layer donors and the Friedel oscillations surrounding them. The atomic corrugation has been filtered out. The amplitude of the height profile of the first layer Si donor is stronger than the second layer, both at the center of the feature and at the first minimum.

The Friedel oscillations are visibly stronger around the donors labeled 1 compared to those labeled 2, as shown in Fig. 3, which shows the radial height profiles around our assigned first- and second-layer Si donor, where the atomic lattice has been filtered out. This leads us to the conclusion that the donors marked with 1 are located closer to the surface than the donors marked with 2.

We identified the features labeled 1 as Si donors located in the first layer (one layer below the surface) and the features labeled 2 as Si donors located in the second layer. These features are equally frequent in our images. A detailed justification for this assignment is given below.

2. Surface layer Si donor

Figure 4(a) shows a $2.5 \times 2.5 \text{ nm}^2$ STM image of a surface Si donor obtained at a bias voltage of –3.0 V and a set-point current of 50 pA. The contrast at the location of the feature is strong, showing an upward tip movement of around 200 pm with respect to the corrugation. At this voltage, we reason that the Si donor in the surface is negatively charged (Si^-), meaning that its dangling bond is filled with two electrons. Such a state has been observed for Si donors in GaAs, where it was attributed to a DX^- -like state [7,49]. During filled-state imaging, electrons are pulled from this dangling bond and quickly replenished from the surrounding 2DEG. Because the dangling bond is highly localized with a strong contrast, the contrast it shows is actually a convolution of the tip and the sample states. This is why the feature is not perfectly symmetrical and instead its exact shape depends on the used tip (see Supplemental Material Fig. S1). The highly localized contrast is confirmed by the simulated STM image derived from DFT calculation on a Si^- in the surface, which is shown as in inset in Fig. 4(a). The contrast of this image ranges from blue (low) to white to red (high).

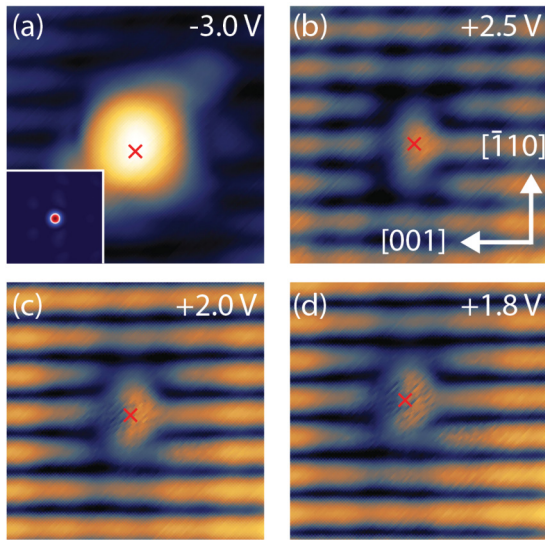


FIG. 4. $2.5 \times 2.5 \text{ nm}^2$ images of a Si donor in the surface layer obtained at a bias voltage of -3.0 V (a), $+2.5 \text{ V}$ (b), $+2.0 \text{ V}$ (c), and $+1.8 \text{ V}$ (d). The red cross marks the location of the Si donor. All images were obtained with a set point current of 50 pA . The inset in (a) shows a $2.5 \times 2.5 \text{ nm}^2$ simulated STM image of a Si^- atom in the surface of ALAs.

Figures 4(b)–4(d) show $2.5 \times 2.5 \text{ nm}^2$ STM images of a surface Si donor obtained at a bias voltage of $+2.5 \text{ V}$, $+2.0 \text{ V}$, and $+1.8 \text{ V}$ respectively. In Fig. 4(b), a reduction of the corrugation contrast is visible on the atoms around the feature, with a separate contrast spreading from single Al lattice site in the $[\bar{1}10]$ and $[1\bar{1}0]$ direction. In Fig. 4(c), the edges of this contrast bend in the $[001]$ direction, creating a double lobed shaped. The two lobes lie directly on As corrugation sites. In Fig. 4(d) the overall strength of the contrast with respect to the corrugation decreases, and some light switching of the contrast can be observed at the location of the two lobed feature. At the positive voltages the Si donor state is pulled above the Fermi level due to TIBB, and as a result is positively charged (Si^+). The symmetry plane of the feature along the $[001]$ crystal axis lies on a C_3 surface state, indicating that the feature is located in an even layer and since it is the only donor showing a drastically different contrast we argue that this is a Si donor in surface plane.

3. First layer Si donor

Si acting as a donor in ALAs means that the Si is substitutionally incorporated at an Al site. At large negative voltages, the As sublattice is imaged and the atomic corrugation consists of the $A_{4,5}$ states. At the location of a Si donor, a depression of around 0.1 \AA is observed, localized on the site of a single As atom as seen in Fig. 5(a). This could indicate a physical depression of the surface at this location or a reduction in the LDOS. Because of the large bias voltage, we expect this to be a topographical effect. This is confirmed by our DFT calculations, which indicate a 0.2 \AA downward movement of the surface As atom chemically bound to the Si donor (See Supplemental Material Fig. S6). Around it, a slight increase of the contrast is observed. At -3.0 V , the

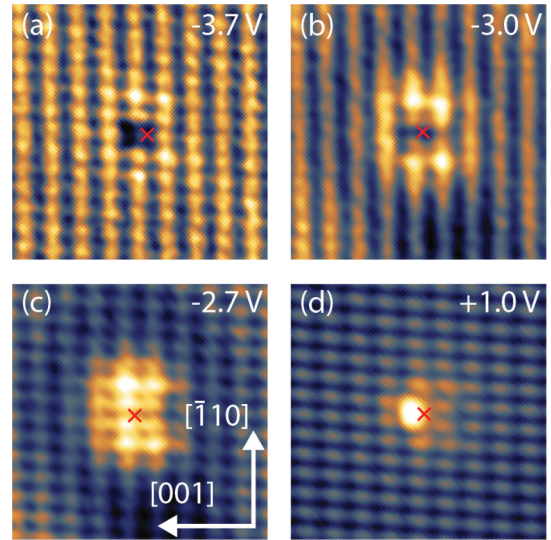


FIG. 5. $4.5 \times 4.5 \text{ nm}^2$ images of a first layer Si donor obtained at a bias voltage of -3.7 V (a), -3.0 V (b), -2.7 V (c) and $+1.0 \text{ V}$. The red cross marks the location of the Si donor in each of the images. All images were obtained with a set-point current of 50 pA .

corrugation is mainly due to the A_5 states. The depression diminishes in strength and the bright contrast surrounding it increases in strength as shown in Fig. 5(b). A ring of dark contrast now surrounds the donor, as a result of the Friedel oscillations. In Fig. 5(a), due to band bending, the amount of electrons in the accumulation layer is much higher, resulting in a very short screening length, effectively removing the Friedel oscillations. At a bias voltage of -2.7 V , the feature contains two prominent lines of bright contrast along the $[001]$ direction, with two rows of less bright contrast in between them, as shown in Fig. 5(c). The corrugation now consists of mainly A_5 and C_3 states, resulting in 2D corrugation. In between these two lines, the image looks brighter than the background lattice but less bright than the two lines. Around the feature, a charge density oscillation is visible. Figure 5(c) shows (at the short range) a striking similarity with a Si donor in GaAs imaged by Feenstra *et al.* [4]. At this voltage, we reason that the shallow Si donor is neutral, d^0 , since the downward bend bending causes the donor level to be well below the Fermi level. However, due to the tip-induced accumulation layer, there will be an interplay between the extra electron from the Si donor and the 2DEG accumulation layer. This leads to a localized neutral donorlike state close to the Si atom, which smoothly transitions into Friedel oscillations due to the tip-induced accumulation layer at longer range. Measuring at positive bias (empty state) voltage of $+1.0 \text{ V}$, the corrugation is dominated by the C_3 and C_4 surface resonances. The Si donor now shows an enhanced contrast at two Al sites, but some of the anisotropic two-line shape from Fig. 5(c) remains. At this voltage, the Si donor level is pulled above the Fermi level, causing the Si donor to be ionized (d^+). This is confirmed with larger scale positive bias images, where disks of ionization are visible around Si donors due to the TIBB ionizing the donor [6] (see Supplemental Material Fig. S2).

The observed contrast at -2.7 V is mirror symmetric, with the mirror axis parallel to the $[001]$ direction. The mirror axis

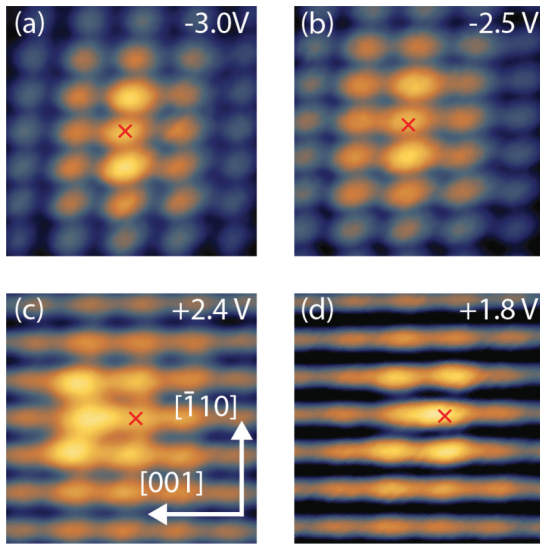


FIG. 6. $2.5 \times 2.5 \text{ nm}^2$ images of a second layer Si donor obtained at a bias voltage of -3.0 V (a), -2.5 V (b), $+2.4 \text{ V}$ (c) and $+1.8 \text{ V}$ (d). The red cross marks the location of the Si donor in each of the images. All images were obtained with a set point current of 50 pA .

lies in between two C_3 states, which means that the Si donor is located an odd amount of layers below the surface. This is also the feature with the strongest Friedel oscillations that has this symmetry and, because the strength of the Friedel oscillations increases when a donor is located closer to the surface, we can conclude that the donors marked with 1 are Si donors one layer below the surface. The apparent discrepancy regarding the symmetry at -3.7 and -3.0 V can be explained by considering that the C_3 states are not visible at these voltages. Instead the contrast contains only A_4 and A_5 states which are centered above the As sites in both $[001]$ and $[\bar{1}10]$ directions, meaning that the mirror axis of a feature in an even layer should lie *on* a corrugation row in the $[001]$ direction. This is indeed what we observe in Figs. 5(a) and 5(b).

4. Second layer Si donor

A Si atom in the second layer below the surface shows a two-lobed structure in filled-state imaging as shown in Figs. 6(a) and 6(b). The lobes are located along the $[\bar{1}10]$ and the feature is mirror symmetric with respect to the $[001]$ axis. In between the two lobes, the feature shows a lower brightness. When the C_3 surface state is contributing to the contrast for filled-state imaging conditions (-3.0 , -2.5 V), the location of the mirror axis is *on* a C_3 line, indicating that the Si atom is located in an even layer (0, 2, 4 layers below the surface), where the Al atoms lie directly below the C_3 lines. In Sec. III B 1, we reasoned that, based on the Friedel oscillation amplitude, feature 2 is located deeper than feature 1, leading to the conclusion that the Si donor is located two layers below the surface. Changing the bias voltage at filled-state imaging conditions has no effect on the shape of the feature as can be seen when comparing Figs. 6(a) and 6(b). At this voltage, there is again the interplay between the single electron on the neutral donor, d^0 , and the surrounding 2DEG in the accumulation layer, leading to a superposition

of the neutral donor image near the Si atom and the Friedel oscillations.

At a positive bias of $+2.4 \text{ V}$, Fig. 6(c), the Si donor shows enhanced contrast on two lines in the $[\bar{1}10]$ direction, with the half facing in the $[001]$ direction having brighter contrast. The contrast surrounding these two lines is slightly brighter than the background. The brightest part of the feature is located in the $[001]$ direction with respect to the location of the Si atom. In Fig. 6(d), the same feature is imaged with a bias voltage of $+1.8 \text{ V}$. Now the brightest part of the feature has shifted to right above the Si atom. Again, at positive voltages the Si donor is pulled above the Fermi level and is positively charged as a result (d^+). Si donors in the third layer below the surface show a very similar structure in terms of symmetry and shape to Si donors in the first layer, but their overall contrast (and Friedel oscillations) is weaker and the contrast is less localized. The same holds for the Si donor that is located four layers below the surface, when comparing it to the Si donor located two layers below the surface (See Supplemental Material Figs. S3 and S4). In general, we can say that the observed contrast of the Si donors alternates for even and odd layers (excluding the surface).

C. DFT

In parallel with STM experiments, DFT calculations were performed on the Si-doped AIAs system. Figure 7(a) shows the calculated band structure of the (110) surface of an intrinsic AIAs slab. In Fig. 7(b), the isolated impurity state introduced by the donor in the surface can be observed below the bottom of the conduction band near the Fermi level. Since these calculations are performed for the neutral donor case (d^0), the Fermi level is pinned by the defect state, which is half occupied. In Fig. 7(c), the band structure for a Si donor one layer below the surface can be observed. In this case, the impurity band can still be observed below the bottom of the conduction band around the Fermi energy, but it is much shallower and the band displays a small dispersion. Consequently, the impurity state wave function has a greater extension in comparison with the previous case, as can be appreciated in Fig. 9. Similar trends are observed when the donor is placed further below the surface, with the impurity state getting consistently closer to the bottom of the conduction band (see Supplemental Material Fig. S5). This trend of the impurity band getting closer to the bottom band with increasing depth can qualitatively be compared with the experimental results. An experimental indication of the donor-induced level can be obtained from Fig. S2, which shows ionization rings around Si donors at various depths below the surface. The ionization rings indicate how close the tip needs to be to cause enough TIBB to ionize the Si donors. TIBB is stronger near the apex of the tip, so the closer the ionization ring is to the donor, the deeper the donor state is located in the AIAs gap. Figure 8 shows a plot of one over the radius of the ionization rings as measured from the center of the donor to the edge of the ring in the $[00\bar{1}]$ direction for different donor depths. We plotted the inverse of the radius to make comparison with calculated energies more convenient. From this, it can be seen that the ionization ring radius of the surface layer Si donor is much smaller than the ones below the surface, which show about

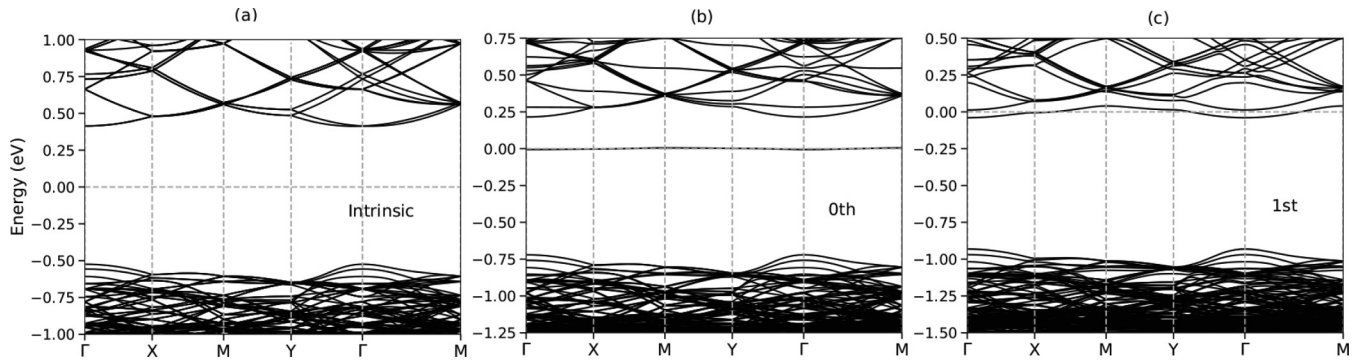


FIG. 7. DFT band structure of a pristine (110) AlAs slab (a) and a Si-doped slab, with the Si donor located at the surface layer (b) and the first layer below the surface (c). The Fermi energy is set to zero in all cases. The impurity state introduced by the Si donor can be observed in the band gap, just below the bottom of the conduction band around zero energy.

the same size. The inverse radius of the second-layer Si donor shows a slight increase compared to the first layer, but this is within the uncertainty of the measurement of the radius and atoms or defects nearby might influence the size of the ionization ring radius. The red dots in Fig. 8 mark the energy difference between the Si-induced state and the bottom of the conduction band at the Γ point as a function of Si donor depth. Here it can be seen the Si-induced state lies much deeper in the gap for the surface Si and the Si donors in deeper layers have much lower energies. From this figure, it can be observed that the inverse of the ionization ring radius and the depth of the Si-induced state clearly follow the same trend. The effect that the donor binding energy increases when the donor is located closer to a semiconductor surface has been observed before [45]. An absolute comparison cannot be made here since DFT does give the true quasiparticle energies of the system and extracting the energies from the ionization ring radius requires knowledge of the exact amount of TIBB, which is nearly impossible.

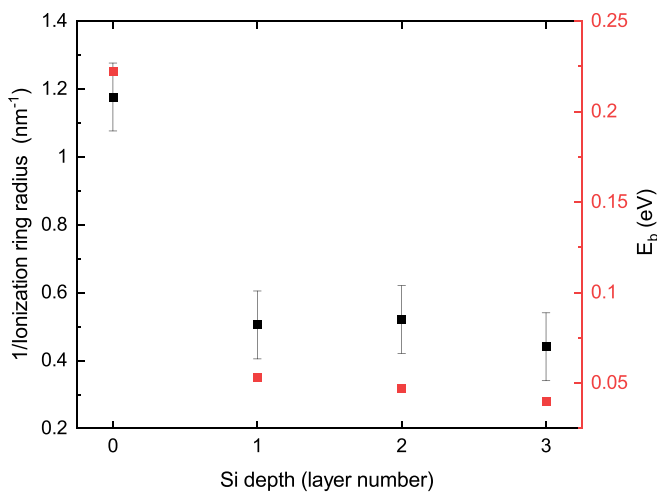


FIG. 8. The inverse of the experimentally obtained ionization ring size as a function of Si donor depth in black including the uncertainties. The red squares indicate the energy difference E_b between the Si-induced state and the bottom of the conduction band at the Γ point as obtained from the DFT calculations.

DFT is also used to simulate constant-height STM images using the Tersoff-Hamann approximation [38]. For this purpose, we compute the LDOS for a small energy window that includes only the defect state. In Fig. 9, we will compare the simulated STM images with the images obtained from experiments. We use empty-state experimental STM images for this comparison. During empty-state imaging (positive bias), TIBB bends the bands upward, causing the Si donor state to be empty (donor is ionized). Electrons are injected

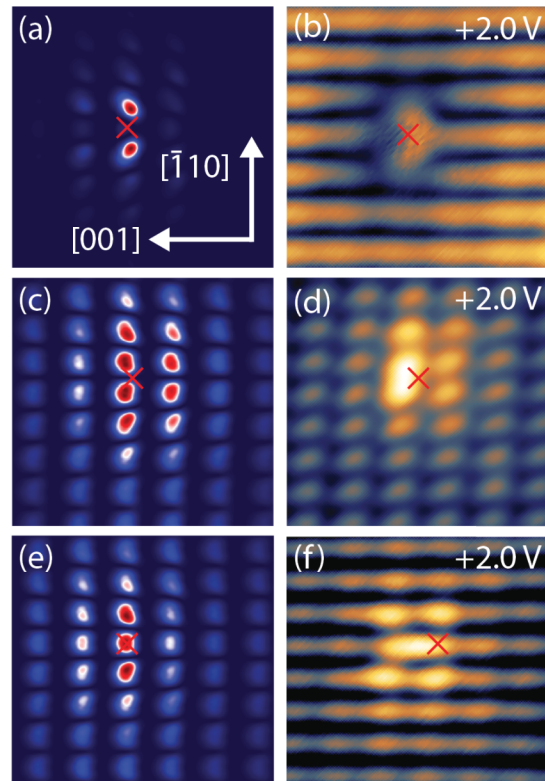


FIG. 9. Simulated STM images from DFT calculations (a), (c), (e) and $2.5 \times 2.5 \text{ nm}^2$ empty state STM images (b), (d), (f) of a Si donor in the surface (a), (b), one layer below (c), (d) and two layers (e), (f) below the surface. The red cross in each image marks the location of the Si donor. The color scale of the simulated STM images ranges from blue (low) to white to red (high).

from the tip into the empty states of the sample, so the higher the LDOS at the location of the tip, the higher the current will be. For this reason, we argue that the comparison of the simulated STM images with the empty-state experimental STM images is valid. Figure 9(a) shows the simulated STM image of a Si donor at the surface. The location of the Si donor in each image is marked with a red cross. At the selected energy range, the LDOS shows a very localized feature near the Si atom. Interestingly, we observe a two-lobed structure near the As atoms neighboring the Si atom in the surface, in striking similarity to the experimental image for positive bias, reproduced in Fig. 9(b). Cross-sectional LDOS images of this defect (done for the small supercells only) and projected density of states calculations (Supplemental Material Fig. S7) show that, in addition to the two features near the As atoms, this state is also composed of a Si *p*-like dangling bond with stronger intensity toward the bulk (therefore, harder to see in STM). Some additional and weaker LDOS can be observed in neighboring corrugation row in the [001] direction. In Fig. 9(b), an empty state STM image of a Si donor in the surface obtained with a bias voltage of +2.0 V is displayed. Additionally, the experimental image shows the C₃ surface states running along the [001] axis (the simulated STM image does not contain the C₃ states because it is taken at a smaller energy window, as we mentioned, including only impurity state). The simulated STM image with an overlay of the atomic lattice can be found in Fig. S8 of the Supplemental Material. For the particular case of the surface donor, we have also performed calculations for a negatively charged impurity. We find a metastable state in which the impurity lies closer to the surface (see Fig. S12 of the Supplemental Material). The total energy of this configuration is about 0.3 eV higher than the most stable configuration, which is identical to the one found for the neutral donor (see Fig. S6). The LDOS profile corresponding to the impurity state found in this metastable configuration, displayed in the inset of Fig. 4(a), displays a strong localization on top of the Si atom, as discussed in Sec. III B 2. Such a metastable configuration is not found in the neutral case.

Figure 9(c) shows a simulated STM image of a Si donor one layer below the surface. The Si donor shows an enhanced LDOS at multiple rows of surface Al atoms in the $[\bar{1}10]$ direction, with the stronger features being concentrated on three of these rows. The middle row shows the strongest LDOS at four Al sites, of which the middle two show the highest brightness. The neighboring corrugation row in the [00 $\bar{1}$] direction shows the second-highest LDOS, with again four sites appearing brighter, of which the middle two the most. The whole feature is mirror symmetric with respect to the [001] axis, with the mirror plane located in between two surface Al atoms. This defect state feature can be rationalized as a product between a delocalized Al-like conduction band surface state and an envelope function that imposes localization near the Si donor. The apparent size of this envelope function is consistent with the average donor bulk Bohr radius of ≈ 13 Å (Supplemental Material Fig. S9) obtained from a hydrogenic model within effective mass theory. In Fig. 9(d), an empty state STM image of a Si donor one layer below the surface is displayed [the same image as in Fig. 6(d)]. Comparing this image with the simulated STM image obtained from DFT calculations in

Fig. 9(c), a very similar structure is observed. Both show enhanced LDOS at three surface Al rows in the $[\bar{1}10]$ direction, with the middle one having the largest LDOS. The asymmetry on the LDOS brightness of the neighboring Al rows is also observed, with four Al sites showing enhancement in the row in the [001] direction and only two sites showing strong enhancement in the [00 $\bar{1}$] direction. This provides further confirmation that the Si donor imaged in Fig. 9(d) is located one layer below the surface and shows that the DFT calculations provide a successful method to simulate STM images.

The Si donor located two layers below the surface [Fig. 9(e)] follows the same trend (enveloped Al surface states), showing an enhancement of the LDOS at three Al surface rows in the $[\bar{1}10]$ direction. Again, the middle one shows the strongest brightness, localized on three Al atoms. The same goes for its two neighboring rows, with the neighbor in the [001] direction appearing slightly brighter than the one in the [00 $\bar{1}$] direction. The whole feature is mirror symmetric with respect to the [001] axis, with the mirror plane going through the central Al row. The comparison between Figs. 9(e) and 9(f) (experiment) again shows an excellent match. Both features are mirror symmetric with respect to the [001] axis, with the mirror plane located on the central Al row, which matches the idea that the Si donor is located directly below a surface Al site in an even layer. In both simulated and experimental images, the middle row is the brightest. The contrast of the Si atom three layers below the surface is shown in Supplemental Material Fig. S13. Overall, there is strong agreement between the simulated and experimental STM images for Si donors in the top four layers of the AIAs (110) surface. In the Supplemental Material, we provide extra theoretical LDOS plots showing cross-sectional features of the defect states contributing to the STM images (done for the small supercells only). In these plots, the interplay between defect and surface states is elucidated.

IV. CONCLUSIONS

We observed Si donors in multiple layers of the AIAs (110) surface. We identified Si donors up to four layers below the surface based on the symmetry and strength of their contrast. Our experimental results and simulated images are mutually supported for donors in the top three layers of AIAs (110) surfaces. This agreement provides a good basis for further exploring the combined STM measurements with DFT calculations on donorlike systems. The trend observed in the band-structure calculations for the energetic position of the Si-induced state below the conduction band for Si atoms in different layers is also observed in the STM measurements. The induced state of the surface Si is much deeper than the state for Si donors deeper below the surface and for Si donors below the surface the energy difference between the bottom of the conduction band slowly decreases. Interestingly, the short-range character of the Si defect LDOS in AIAs is not very different from Si in GaAs, but in AIAs the short-range, localized character of the Si atoms can be observed. Finally, the similarities between the STM images of Si impurities in the (110) surfaces of AIAs and GaAs, despite their different band-gap nature in bulk form, may be related to the valley composition of the conduction band edge for the surface. As

we have discussed above, in AIAs the bottom of the conduction band, originally at the X point of the bulk BZ is folded into the Γ point of the surface BZ, resulting in a direct band gap. In GaAs, the gap is already direct in bulk form and lies at the Γ point. Therefore, the two materials should display the same valley physics at this surface, as the donor state wave functions should result from linear combinations of states near the bottom of the conduction band. The four-layer cycle interference pattern of the donor contrast of the surface, as observed for P in Si, is not observed for Si in AIAs. Instead,

the donor contrast varies only between even and odd layers because of the different coupling to surface states depending on the symmetry of the different layers.

ACKNOWLEDGMENTS

We acknowledge financial support from Brazilian funding agencies CAPES, CNPq, FAPERJ, INCT-Nanomateriais de Carbono and INCT-Informação Quântica.

-
- [1] P. M. Koenraad and M. E. Flatté, *Nat. Mater.* **10**, 91 (2011).
- [2] J. F. Zheng, X. Liu, N. Newman, E. R. Weber, D. F. Ogletree, and M. Salmeron, *Phys. Rev. Lett.* **72**, 1490 (1994).
- [3] C. Domke, P. Ebert, and K. Urban, *Surf. Sci.* **415**, 285 (1998).
- [4] R. M. Feenstra, G. Meyer, F. Moresco, and K. H. Rieder, *Phys. Rev. B* **66**, 165204 (2002).
- [5] S. Loth, M. Wenderoth, K. Teichmann, and R. G. Ulbrich, *Solid State Commun.* **145**, 551 (2008).
- [6] K. Teichmann, M. Wenderoth, S. Loth, R. G. Ulbrich, J. K. Garleff, A. P. Wijnheijmer, and P. M. Koenraad, *Phys. Rev. Lett.* **101**, 076103 (2008).
- [7] J. K. Garleff, A. P. Wijnheijmer, C. N. Denden, and P. M. Koenraad, *Phys. Rev. B* **84**, 075459 (2011).
- [8] E. P. Smakman and P. M. Koenraad, *J. Phys.: Condens. Matter* **27**, 154201 (2015).
- [9] E. P. Smakman, J. van Bree, and P. M. Koenraad, *Phys. Rev. B* **87**, 085414 (2013).
- [10] See Supplemental Material at <http://link.aps.org/supplemental/10.1103/PhysRevB.104.125433> for additional supporting figures.
- [11] P. M. Mooney, *J. Appl. Phys.* **67**, R1 (1990).
- [12] B. Koiller, X. Hu, and S. Das Sarma, *Phys. Rev. Lett.* **88**, 027903 (2001).
- [13] J. Salfi, J. A. Mol, R. Rahman, G. Klimeck, M. Y. Simmons, L. C. L. Hollenberg, and S. Rogge, *Nat. Mater.* **13**, 605 (2014).
- [14] V. Berkovits, I. Makarenko, T. Minashvili, and V. Safarov, *Solid State Commun.* **56**, 449 (1985).
- [15] C. B. Duke, *Chem. Rev.* **96**, 1237 (1996).
- [16] G. P. Srivastava, *Rep. Prog. Phys.* **60**, 561 (1997).
- [17] A. Baena, A. L. Saraiva, M. G. Menezes, and B. Koiller, *Europhys. Lett.* **116**, 20002 (2016).
- [18] A. L. Saraiva, J. Salfi, J. Bocquel, B. Voisin, S. Rogge, R. B. Capaz, M. J. Calderón, and B. Koiller, *Phys. Rev. B* **93**, 045303 (2016).
- [19] C. Asplund, S. Mogg, G. Plaine, F. Salomonsson, N. Chitica, and M. Hammar, *J. Appl. Phys.* **90**, 794 (2001).
- [20] T. Yao, Y. Okada, S. Matsui, H. Nagase, and K. Ishida, *J. Appl. Phys.* **62**, 1925 (1987).
- [21] I. Reshina and R. Planel, *Semiconductors* **32**, 745 (1998).
- [22] R. B. Capaz, K. Cho, and J. D. Joannopoulos, *Phys. Rev. Lett.* **75**, 1811 (1995).
- [23] M. Diarra, Y.-M. Niquet, C. Delerue, and G. Allan, *Phys. Rev. B* **75**, 045301 (2007).
- [24] G. Bastard, *Wave Mechanics Applied to Semiconductor Heterostructures* (Les Editions de Physique, Les Ulis Cedex, France, 1988).
- [25] I. Vurgaftman, J. R. Meyer, and L. R. Ram-Mohan, *J. Appl. Phys.* **89**, 5815 (2001).
- [26] P. Giannozzi, S. Baroni, N. Bonini, M. Calandra, R. Car, C. Cavazzoni, D. Ceresoli, G. L. Chiarotti, M. Cococcioni, I. Dabo, A. Dal Corso, S. De Gironcoli, S. Fabris, G. Fratesi, R. Gebauer, U. Gerstmann, C. Gougoussis, A. Kokalj, M. Lazzeri, L. Martin-Samos *et al.*, *J. Phys.: Condens. Matter* **21**, 395502 (2009).
- [27] P. Giannozzi, O. Andreussi, T. Brumme, O. Bunau, M. B. Nardelli, M. Calandra, R. Car, C. Cavazzoni, D. Ceresoli, M. Cococcioni *et al.*, *J. Phys.: Condens. Matter* **29**, 465901 (2017).
- [28] W. Kohn, Y. Meir, and D. E. Makarov, *Phys. Rev. Lett.* **80**, 4153 (1998).
- [29] J. F. Dobson and B. P. Dinte, *Phys. Rev. Lett.* **76**, 1780 (1996).
- [30] Y. Andersson, D. C. Langreth, and B. I. Lundqvist, *Phys. Rev. Lett.* **76**, 102 (1996).
- [31] A. Dal Corso, *Comput. Mater. Sci.* **95**, 337 (2014).
- [32] G. Prandini, A. Marrazzo, I. E. Castelli, N. Mounet, and N. Marzari, *npj Comput. Mater.* **4**, 72 (2018).
- [33] K. Lejaeghere, G. Bihlmayer, T. Björkman, P. Blaha, S. Blügel, V. Blum, D. Caliste, I. E. Castelli, S. J. Clark, A. Dal Corso, S. de Gironcoli, T. Deutsch, J. K. Dewhurst, I. Di Marco, C. Draxl, M. Dułak, O. Eriksson, J. A. Flores-Livas, K. F. Garrity, L. Genovese *et al.*, *Science* **351**, aad3000 (2016).
- [34] H. J. Monkhorst and J. D. Pack, *Phys. Rev. B* **13**, 5188 (1976).
- [35] J. M. Soler, E. Artacho, J. D. Gale, A. García, J. Junquera, P. Ordejón, and D. Sánchez-Portal, *J. Phys.: Condens. Matter* **14**, 2745 (2002).
- [36] N. Troullier and J. L. Martins, *Phys. Rev. B* **43**, 1993 (1991).
- [37] J. P. Perdew and A. Zunger, *Phys. Rev. B* **23**, 5048 (1981).
- [38] J. Tersoff and D. R. Hamann, *Phys. Rev. B* **31**, 805 (1985).
- [39] J. R. Chelikowsky and M. L. Cohen, *Phys. Rev. B* **20**, 4150 (1979).
- [40] G. J. de Raad, D. M. Bruls, P. M. Koenraad, and J. H. Wolter, *Phys. Rev. B* **66**, 195306 (2002).
- [41] A. R. Lubinsky, C. B. Duke, B. W. Lee, and P. Mark, *Phys. Rev. Lett.* **36**, 1058 (1976).
- [42] D. J. Chadi, *Phys. Rev. B* **19**, 2074 (1979).
- [43] A. Kahn, *Surf. Sci.* **168**, 1 (1986).

- [44] R. M. Feenstra, J. M. Woodall, and G. D. Pettit, *Phys. Rev. Lett.* **71**, 1176 (1993).
- [45] A. P. Wijnheijmer, J. K. Garleff, K. Teichmann, M. Wenderoth, S. Loth, R. G. Ulbrich, P. A. Maksym, M. Roy, and P. M. Koenraad, *Phys. Rev. Lett.* **102**, 166101 (2009).
- [46] J. Friedel, *Il Nuovo Cimento (1955-1965)* **7**, 287 (1958).
- [47] M. C. M. M. van der Wielen, A. J. A. van Roij, and H. van Kempen, *Phys. Rev. Lett.* **76**, 1075 (1996).
- [48] M. C. M. M. Van der Wielen, Study of imperfections near the cleaved GaAs (110) surface by low-temperature scanning tunneling microscopy, Ph.D. thesis, Katholieke Universiteit Nijmegen, 1998.
- [49] Z. Yi, Y. Ma, and M. Rohlfing, *J. Phys. Chem. C* **115**, 23455 (2011).